Pergamon

Int. J. Heat Mass Transfer. Vol. 40, No. 7, pp. 1677–1686, 1997

0017–9310/97 $17.00+0.00

PII: S0017-9310(96)00219-0

Numerical study of a backward-facing step with uniform normal mass bleed

YUE-TZU YANG and CHUNG-LUN KUO

Department of Mechanical Engineering, National Cheng Kung University, Tainan, Taiwan 701, Republic of China

(*Received* 8 *January* 1996)

Abstract—This study presents the numerical predictions of the fluid flow characteristics within the recirculation zone for a backward-facing step with uniform normal mass bleed. The turbulent governing equations are solved by a control-volume-based finite-difference method with power-law scheme. A new turbulence model is proposed to describe the turbulent structure. Non-uniform staggered grids are used. The parameters studied include entrance Reynolds number (Re), and the velocity of the normal mass bleed (V_s). The channel expansion ratio $ER = 1.3$, and the working medium is air. The numerical results show the uniform normal mass bleed suppresses the reverse horizontal velocity, turbulence intensity, and Reynolds shear stress within the recirculation zone. The attachment point extends to downstream. Better computational predictions are obtained with the new turbulence model by the introduction of the Kolmogorov velocity scale, $U_\varepsilon = (\nu\varepsilon)^{1/4}$ instead of friction velocity U_τ. Copyright © 1996 Elsevier Science Ltd.

INTRODUCTION

The flow over a backward-facing step produces a separated-reattaching which is an important process in a large number of practical engineering configurations, including airfoils, electrical devices, diffusers, and combustors. Although such a flow pattern has been studied by many investigators, a detailed mechanism of backward-facing step with uniform normal mass bleed was seldom found. Abbort and Kline [1] used a visualisation technique involving dye in measuring the velocity profiles of water flowing over single and double steps. The turbulent flows pattern and reattachment length were found to be unchanged with Re_h (based on the step-height H) ranging from 10000–125000, and for a variation in the inlet turbulence intensity from approximately 1 to 18% of the mainstream velocity. Aung [2] indicated that the initial boundary-layer thickness was inversely proportional to the reattachment length, and the streamline curvature caused the streamlines upstream of the step to become essentially parallel to the wall. It showed that the numerical calculation of flows over steps may need to begin upstream of the step at least in the case of low Re_h flows to include this effect. Armaly *et al.* [3] used laser doppler anemometry to probe the velocity profiles and the reattachment length of a laminar and turbulent duct flow with a backward-facing step, and showed the reattachment length will be different for different Reynolds numbers. Eaton and Johnston [4] summarized five principal independent parameters influencing the reattachment length, which include: the initial boundary-layer state, the initial boundary-layer thickness, the freestream turbulence, the pressure gradient and the aspect ratio. Kim *et al.* [5] indicated that turbulent intensities and shear stress reach maximum in the reattachment zone, followed by rapid decay near the surface after reattachment.

Schetz and Nerney [6] experimentally investigated the turbulent boundary layer with injection. The experiments reported that the velocity and turbulence intensity in the turbulent boundary layer increased with increasing rate of injection. Groot [7] used laser Doppler anemometry to probe the mixing turbulent flow over a two-dimensional backward-facing step with side-wall injection. It showed that the side-wall injection suppressed the reverse horizontal velocity, turbulence intensity and Reynolds shear stress, but the reattachment length was insensitive to the side-injection. Lin *et al.* [8] discussed the effects of buoyancy-assisting and indicated that the influence of the buoyancy force on the velocity distribution is more pronounced than its influence on the temperature distribution. The buoyancy force significantly changes the shape of the main recirculation region behind the step and causes the reattachment length to decrease as its magnitude increases. Isomoto and Honami [9] installed a two-dimensional cavity or rod upstream of the step in order to change the local turbulence intensity. It showed that the reattachment length has a strong negative correlation with the maximum turbulence intensity near the wall at separation; while the effect of the velocity distribution through the inlet boundary layer on the reattachment process is weak. Turbulence in the entrainment region immediately downstream of the step plays an important role in determining the reattachment length. Oyakawa *et al.* [10] studied the fluid flow and heat transfer characteristics for a backward-facing step by discharging a jet perpendicularly to the main flow. The results

NOMENCLATURE

C_P	pressure coefficient	Xr	flow reattachment length
ER	expansion ratio	y^+	dimensionless distance from the wall, $u_\tau y/\nu$
G	generation rate of turbulent kinetic energy	y^*	dimensionless distance from the wall, $u_\varepsilon y/\nu$.
H	step height		
k	turbulent kinetic energy		
P	pressure		
Re_h	Reynolds number based on step height, $U_0 H/\nu$	Greek symbols	
Re_t	turbulent Reynolds number, $k^2/\nu\varepsilon$	ρ	density
S	source term	κ	Von Karman constant
TI	turbulence intensity	σ	turbulent Prandtl number
U_0	inlet velocity	ν	kinematic viscosity
U_τ	friction velocity	μ	dynamic viscosity
U_ε	Kolmogorov velocity scale, $(\nu\varepsilon)^{1/4}$	τ_w	wall shear stress
		ε	turbulent energy dissipation rate.

showed that the optimum position was at $X_j/H = 2.1$. The augmentation of mean heat transfer coefficients can be as much as 1.6 times the value without jet discharge. The effect of normal mass bleed into the separated-reattaching flow behind a backward-facing step has been investigated experimentally by Yang *et al.* [11] as shown in Fig. 1. Limited data exist for the case where normal injection is applied to the surface and therefore, as a preliminary to looking at a more realistic problem, numerical studies on the effect of a normal injection on the flow field are presented and compared with the only known experimental data of Yang *et al.* [11], by using a standard k–ε turbulence model as well as a new turbulence model.

MATHEMATICAL FORMULATION

The governing equations to be solved are the continuity equation, the time-mean averaged Navier–Stokes equation and the equations of the turbulent kinetic energy k and its dissipation rate ε:

$$\frac{\partial \bar{U}_i}{\partial x_i} = 0 \tag{1}$$

$$\frac{\partial \bar{U}_i}{\partial t} + \bar{U}_j \frac{\partial \bar{U}_i}{\partial x_j} = -\frac{1}{\rho}\frac{\partial \bar{P}}{\partial x_i} + \frac{\partial}{\partial x_j}\left\{\nu\left(\frac{\partial \bar{U}_i}{\partial x_j} + \frac{\partial \bar{U}_j}{\partial x_i}\right) - \overline{u_i u_j}\right\} \tag{2}$$

$$\frac{\partial k}{\partial t} + \bar{U}_j \frac{\partial k}{\partial x_j} = \frac{\partial}{\partial x_j}\left\{\left(\nu + \frac{\nu_t}{\sigma_k}\right)\frac{\partial k}{\partial x_j}\right\} - \overline{u_i u_j}\frac{\partial \bar{U}_i}{\partial x_j} - \varepsilon \tag{3}$$

$$\frac{\partial \varepsilon}{\partial t} + \bar{U}_j \frac{\partial \varepsilon}{\partial x_j} = \frac{\partial}{\partial x_j}\left\{\left(\nu + \frac{\nu_t}{\sigma_\varepsilon}\right)\frac{\partial \varepsilon}{\partial x_j}\right\} - C_{\varepsilon 1}\frac{\varepsilon}{k}\overline{u_i u_j}\frac{\partial \bar{U}_i}{\partial x_j} - C_{\varepsilon 2} f_\varepsilon \frac{\varepsilon^2}{k} \tag{4}$$

where

$$-\overline{u_i u_j} = \nu_t\left(\frac{\partial \bar{U}_i}{\partial x_j} + \frac{\partial \bar{U}_j}{\partial x_i}\right) - \frac{2}{3}k\delta_{ij} \tag{5}$$

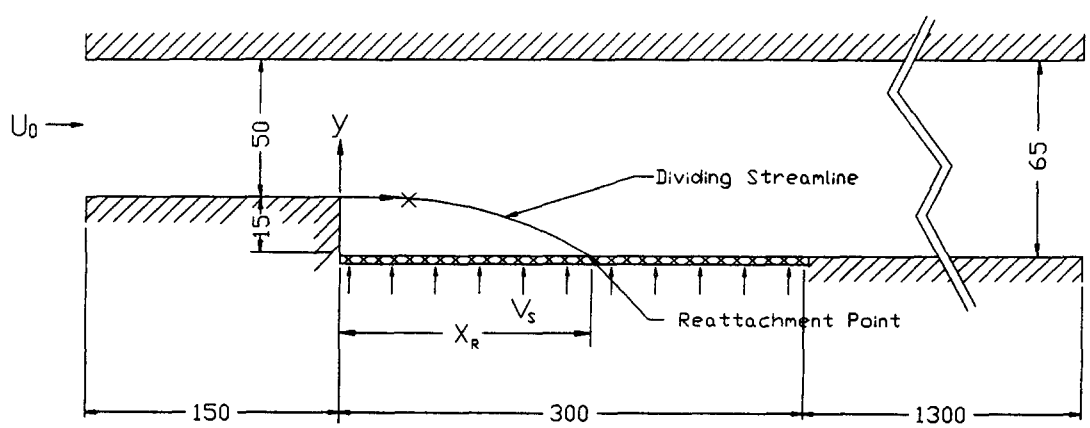

Fig. 1. Physical domain.

$$\nu_t = C_\mu f_\mu \frac{k^2}{\varepsilon} \tag{6}$$

where f_μ and f_ε are the model functions to account for the near-wall and low-Reynolds number effects, and C_μ, $C_{\varepsilon 1}$, $C_{\varepsilon 2}$, σ_k and σ_ε are the model constants.

The steady conservation equations for incompressible two-dimensional Cartesian coordinates mean flow and thermal characteristics of turbulent flow can be written as:

$$\frac{\partial}{\partial x}(\rho U\phi) + \frac{\partial}{\partial y}(\rho V\phi) = \frac{\partial}{\partial x}\left[\Gamma_\phi \frac{\partial \phi}{\partial x}\right] + \frac{\partial}{\partial y}\left[\Gamma_\phi \frac{\partial \phi}{\partial y}\right] + S_\phi \tag{7}$$

where ϕ stands for the dependent variables U, V, k, and ε; U, V, are the local time-averaged velocity in x- and y-directions, respectively; Γ_ϕ and S_ϕ are the corresponding turbulent diffusion coefficient and source term respectively for general variable ϕ. The equations are summarized in Table 1. The turbulent viscosity μ_T and μ_e are expressed as follows:

$$\mu_T = \rho C_\mu f_\mu \frac{k^2}{\varepsilon} \tag{8}$$

$$\mu_e = \mu_l + \mu_T = \mu_l + \rho C_\mu f_\mu \frac{k^2}{\varepsilon} \tag{9}$$

where the model functions and turbulence constant are summarized in Tables 2 and 3.

Table 3. Model constants

	C_μ	C_1	C_2	σ_k	σ_ε
Standard k–ε model	0.09	1.44	1.92	1.0	1.3
New turbulence model	0.09	1.5	1.9	1.4	1.4

Boundary conditions

The computational domain boundaries are shown in Fig. 2. The boundary conditions for the above set of governing equations are:

(1) *Inlet boundary* (A–E). At this boundary, uniform flow conditions are imposed as follows:

$$U = U_{in}, \quad k = k_{in} = TI \cdot U_{in}^2$$

$$\varepsilon = \varepsilon_{in} = \frac{k_{in}^{3/2}}{\lambda D} \tag{10}$$

where TI is the turbulent intensity, λ is the length scale constant, and D is the inlet width.

(2) *Wall boundary.*

(a) Solid wall (A–A'), (A'–B), (B–C) and (D–E). In the standard k–ε model, the near-wall region was simulated by a two zone model, i.e. viscous sublayer and fully turbulent zone, and the wall function method was used to bridge the viscous sublayer, k and ε were handled by the wall function proposed by Launder and Spalding [12]. In the new turbulence model proposed by Abe *et al.* [13] with non-slip boundary

Table 1. Conservation equations†

Equation	ϕ	Γ_ϕ	S_ϕ
Mass	1	0	0
X-momentum	u	μ_e	$-\frac{\partial p}{\partial x} + \frac{\partial}{\partial x}\left[\mu_e \frac{\partial u}{\partial x}\right] + \frac{\partial}{\partial y}\left[\mu_e \frac{\partial v}{\partial x}\right]$
Y-momentum	v	μ_e	$-\frac{\partial p}{\partial y} + \frac{\partial}{\partial x}\left[\mu_e \frac{\partial u}{\partial y}\right] + \frac{\partial}{\partial y}\left[\mu_e \frac{\partial v}{\partial y}\right]$
Turbulent kinetic energy	k	μ_e/σ_k	G-$\rho\varepsilon$
Turbulent energy dissipation rate	ε	μ_e/σ_ε	$\frac{\varepsilon}{k}(C_1 G - C_2 f_\varepsilon \rho\varepsilon)$

† Where $G = \mu_T\{2[(\partial u/\partial x)^2 + (\partial v/\partial y)^2] + (\partial u/\partial y + \partial v/\partial x)^2\}$.

Table 2. Model functions

	Standard k–ε model	New turbulence model
f_μ	1	$f_\mu = \left\{1 - \exp\left(-\frac{y^*}{14}\right)\right\}^2 \left[1 + \frac{5}{R_t^{3/4}} \exp\left\{-\left(\frac{R_t}{200}\right)^2\right\}\right]$
f_ε	1	$f_\varepsilon = \left\{1 - \exp\left(-\frac{y^*}{3.1}\right)\right\}^2 \left[1 - 0.3 \exp\left\{-\left(\frac{R_t}{6.5}\right)^2\right\}\right]$

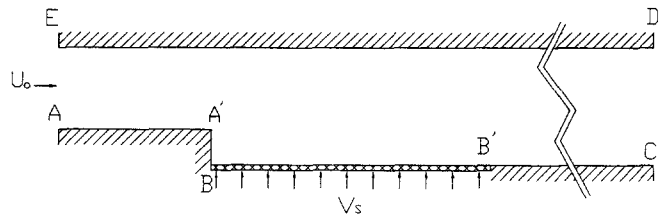

Fig. 2. Coordinate system and boundary conditions of the calculating domain.

conditions:

$$U_w = V_w = k_w = 0 \tag{11}$$

$$\varepsilon_w = \frac{2\nu k_P}{y_P^2}. \tag{12}$$

(b) Porous wall (B–B′).

$$V_{in} = V_s \tag{13}$$

For flow over a porous wall, the wall function is modified to allow for the effect of mass bleed presented by Bradshaw [14]. U_ε is introduced instead of U_τ as following:

$$\frac{2U_\varepsilon}{V_s}\left[\left(1+\frac{UV_s}{U_\varepsilon^2}\right)^{1/2}-1\right]=\frac{1}{\kappa}\ln\left(\frac{U_\varepsilon y}{\nu}\right)+C \tag{14}$$

(3) *Outlet boundary*. The flow field can be regarded as fully developed when the outlet is located far away from recirculation region. The zero normal gradients at the outlet plane is given as:

$$\frac{\partial U}{\partial x}=0, \quad \frac{\partial V}{\partial x}=0. \tag{15}$$

NUMERICAL PROCEDURE

The numerical method used in the present study is based on the SIMPLE algorithm of Patankar [15]. The conservation equations are discretized using a control volume approach based on the finite difference method with power-law scheme. The set of difference equations are solved iteratively using a line by line solution method in conjunction with a tridiagonal matrix form. A nonuniform grid arrangement was used in the present computations. The grid system was suggested with the velocity nodes displaced from scalar nodes. A grid independence test was performed with five different grid sizes (based on the new turbulence model), namely 103×53, 113×63, 122×72, 135×80 and 145×89. The parameters used to check the grid independence of the computational results were the reattachment length (Xr), which has historically been used to assess the overall predictive capability of turbulence models, and the turbulent kinetic energy profiles, as shown in Fig. 3. The calculation solutions appear to be independent of grid distribution of 135×80.

RESULTS AND DISCUSSION

A detailed comparison of the mean horizontal velocity distribution at $U_0 = 20$ m s^{-1} with $V_s = 0$, 0.05, 0.10 and 0.15 m s^{-1} is shown in Fig. 4. At these injection velocities the overall flow structure is reasonably well predicted. It is obvious that the mean velocity is reduced near the wall as the injection velocity is increased. As might be expected, the agreement is much better towards the outside recirculation region. It indicates that curves for $V_s = 0$, 0.05, 0.10 and 0.15 m s^{-1} are almost coincident at 0.2 Xr. The velocity vector plots of Fig. 5 provide an overall view of the flow. Streamlines of the flow field for different injection velocities are plotted in Fig. 6. The predictions of flow reattachment length with standard k–ε turbulence model and a new turbulence model are presented in Fig. 7. The predictions of flow reattachment length are seen to be in good agreement with the experiments within 4% discrepancy, using a new turbulence model. The static pressure coefficient distribution are presented in Fig. 8. It is indicated that the static pressure increases significantly in the front of the recirculation region as the injection rate increases. The steep pressure gradient occurs at the reattachment point. The results show the relation of C_P and Xr/H respectively. It can be seen that variation of C_P tends to be insensitive when $U_0 = 60$ m s^{-1}.

The definition of turbulence intensity is expressed as follows:

$$\text{turbulence intensity} = \left(\frac{\overline{u'^2}+\overline{v'^2}}{2}\right)^{1/2} \tag{16}$$

The effect of normal mass injection through the porous wall on turbulence intensity is more significant than the effect on the mean horizontal velocity as shown in Fig. 9 The turbulence intensity near the porous wall is significantly dampened when the normal injection is increased. It can be seen that the variations of turbulent intensity present almost the same trend in accordance with the experiments of Yang *et al.* [11] and Groot [7]. The reduction of the turbulence intensity is obvious at $X/Xr = 0.2$ and 0.3. The effects of injection velocity on the distribution of Reynolds shear stress at $U_0 = 20$ m s^{-1} is presented in Fig. 10. The experiments show that no obvious change in Reynolds shear stress in the near wall region ($Y/H = -1.0$ to -0.9) at $X/Xr = 0.2$, while the cal-

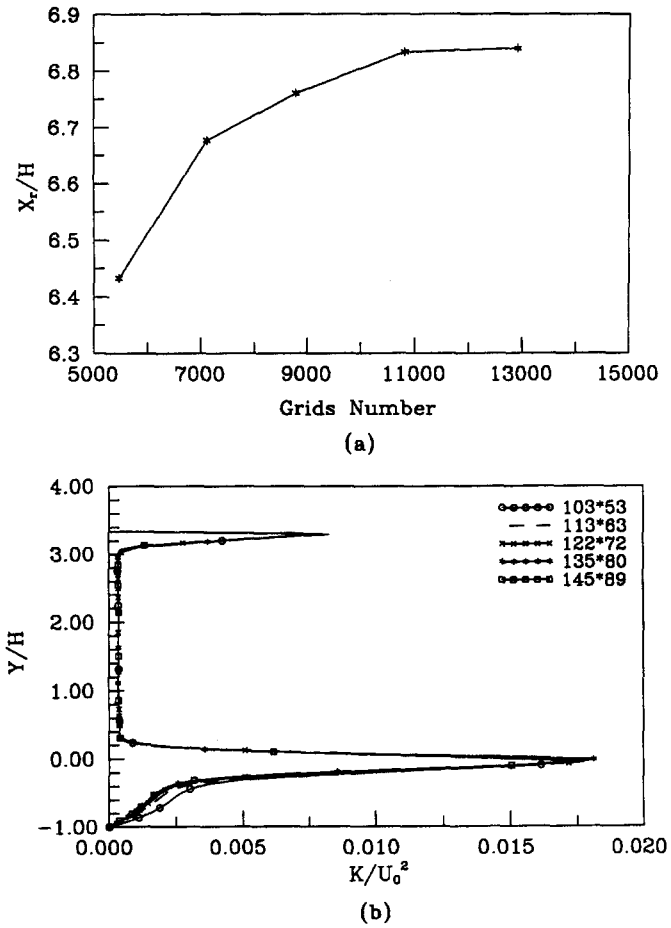

Fig. 3. Effect of grid refinement on (a) reattachment length; (b) turbulent kinetic energy.

culations predict, effectively, the same trend as the experiments. Very near the wall, the experimental instrument was limited. The flow near the wall of the recirculation zone is expected to have a negative dU/dy, therefore it has a negative Reynolds shear stress, the numerical predictions can present this phenomena effectively. This means that the experimental data may be not collected for the near wall region. The effect of injection rate on Reynolds shear stress seems significant in the region of $Y/H = -0.8$ to -0.45, and it decreases as the rate of injection rate increases. The maximum gradients of Reynolds shear stress are located on both boundaries of the shear layer. The effect of normal injection rate on maximum reverse velocity at different cross sections in the recirculating region at $U_0 = 20$ m s^{-1} are shown in Fig. 11. It is clear that the normal injection reduces the maximum reverse velocity occurs at 0.55 Xr in the range of 0.14 U_0–0.20 U_0. The differences occur at the leading part of the flow field. The computational results of the maximum reverse velocity show slightly lower values than the experiments. For the maximum Reynolds shear stress as shown in Fig. 12, the computational results are generally higher than the experimental data of Yang, *et al.* [11]. All corresponding data fall within the envelope, except at $Xr = 0.6$, 0.7 for $V_s = 0$ m s^{-1} and $Xr = 0.8$ for $V_s = 0.05$ m s. In the experiment, the distributions of maximum Reynolds shear stresses are more smooth for the case of $V_s = 0.10$ m s^{-1} and $V_s = 0.15$ m s^{-1}. The maximum Reynolds shear stresses are found to be dampened, due to normal injection.

CONCLUSIONS

The present study provides a new turbulence model which predicts successfully for a backward-facing step with a normal injection. The Kolmogorov velocity scale, $U_\varepsilon = (\nu\varepsilon)^{1/4}$ is introduced, instead of the friction velocity U_τ, to account for the near wall and low-Reynolds number effects. From the computational results, normal injection significantly effect the flow field of the recirculation zone behind the step. The horizontal velocity near the wall in the recirculation zone decreases with increasing the injection rate. With normal injection, both the maximum reverse velocity and reverse flow rate in the recirculation zone are found to be decreased. Certain discrepancies between calculations and the available data may be caused

(a)

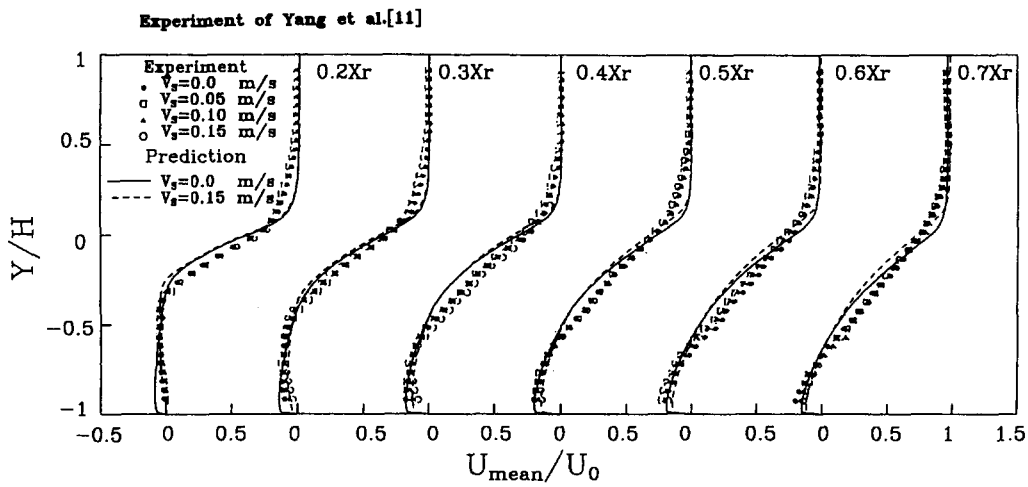

(b)

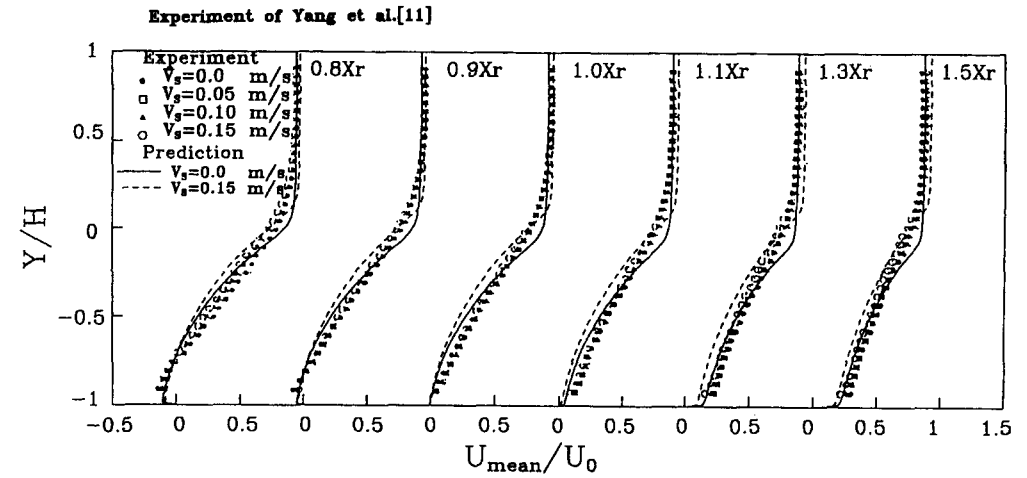

Fig. 4. Effects of the normal injection rate on mean horizontal velocity distribution at $U_0 = 20$ m/s with the new turbulence model (a) $X/Xr = 0.2$, 0.3, 0.4, 0.5, 0.6 and 0.7; (b) $X/Xr = 0.8$, 0.9, 1.0, 1.1, 1.3 and 1.5.

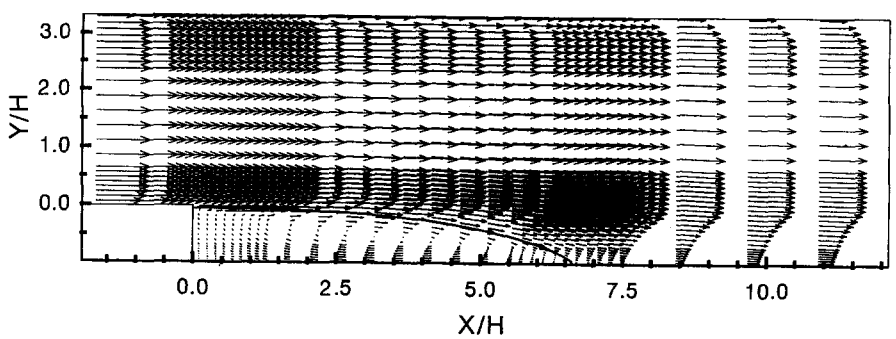

Fig. 5. Velocity vectors of the flowfield with the new turbulence model.

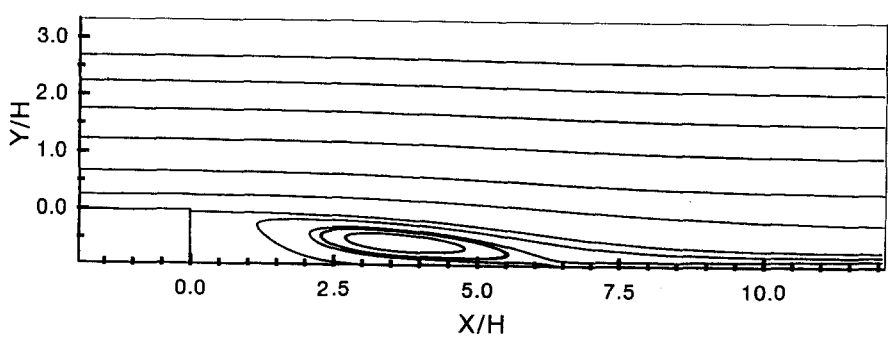

Fig. 6. Streamlines of the flowfield.

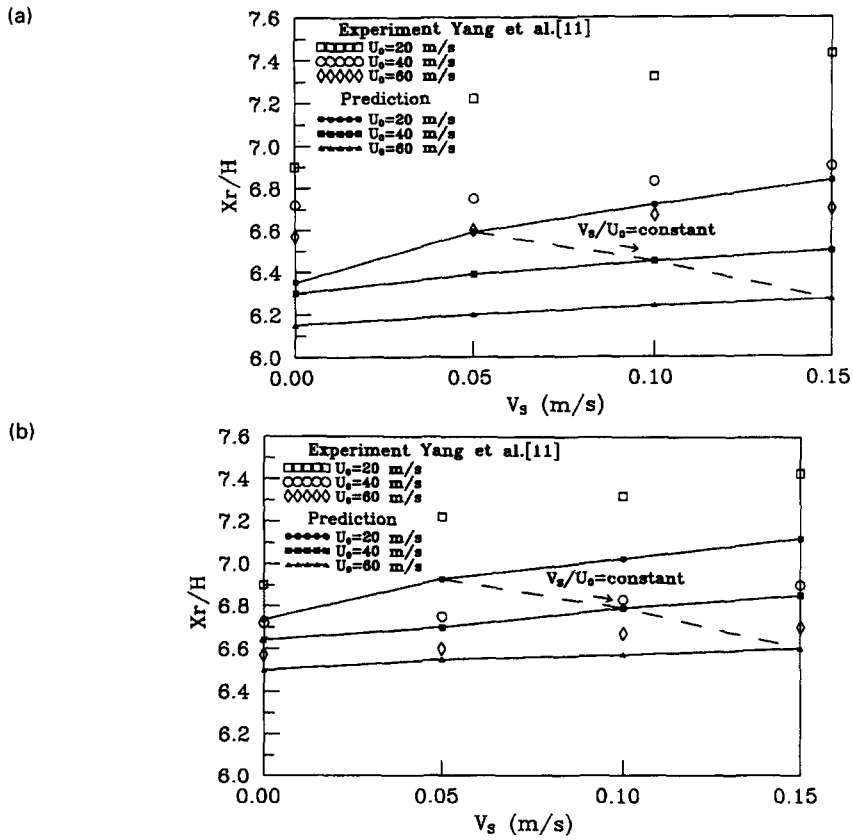

Fig. 7. Effects of normal injection on reattachment length (a) with the standard k–ε turbulence model; (b) with the new turbulence model.

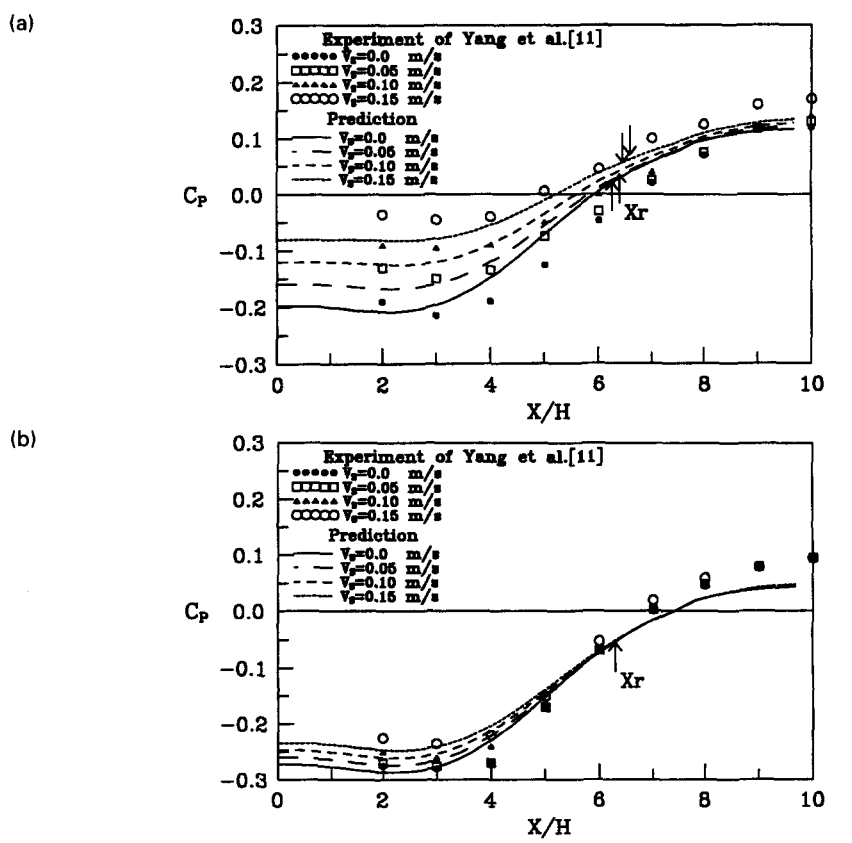

Fig. 8. Static pressure coefficient distribution with various injection rates at (a) $U_0 = 20$ m/s; (b) $U_0 = 60$ m s^{-1}.

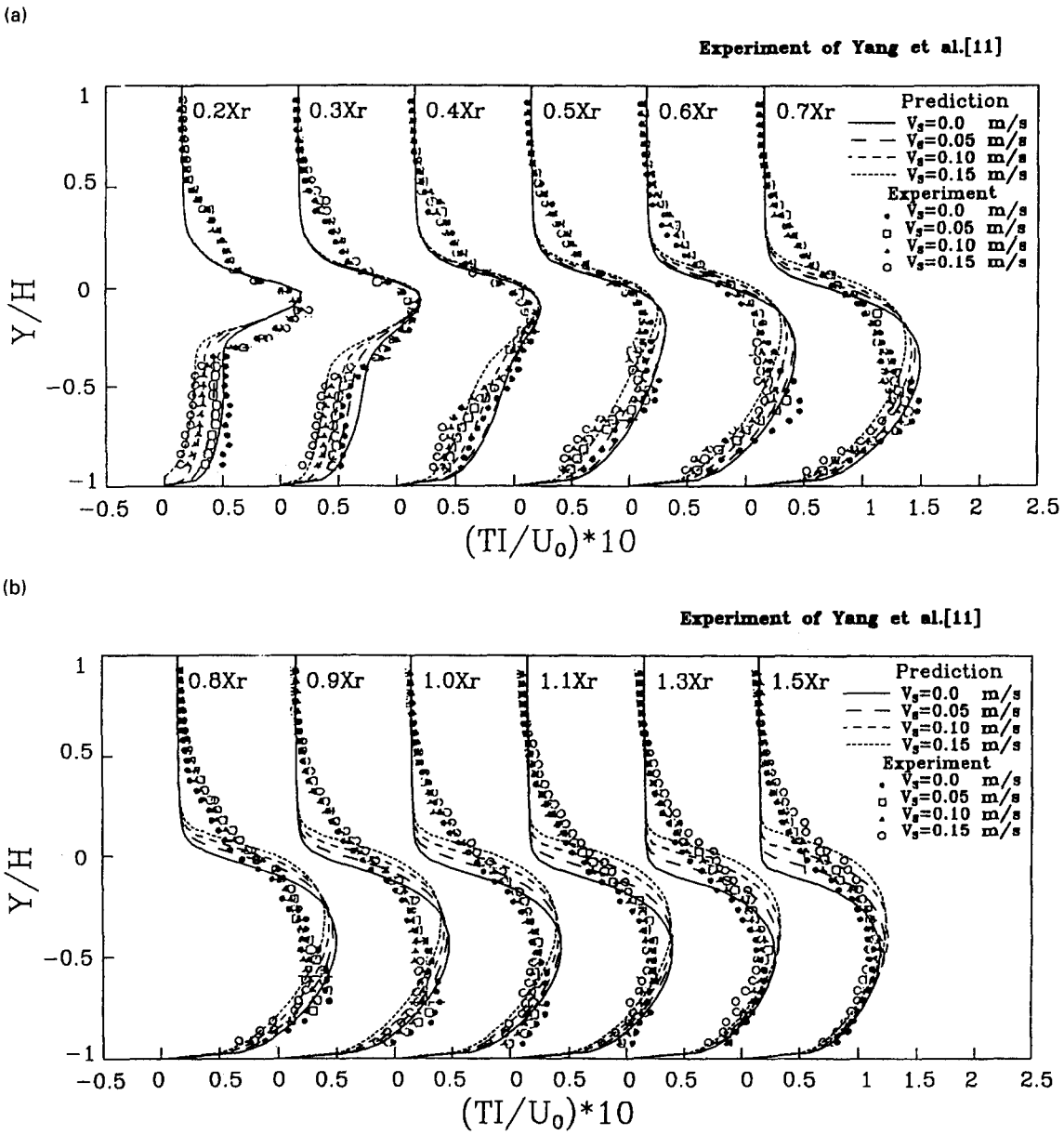

Fig. 9. Effects of the normal injection rate on turbulence intensity distribution at $U_0 = 20$ m s^{-1} (a) $X/Xr = 0.2$, 0.3, 0.4, 0.5, 0.6 and 0.7; (b) $X/Xr = 0.8$, 0.9, 1.0, 1.1, 1.3 and 1.5.

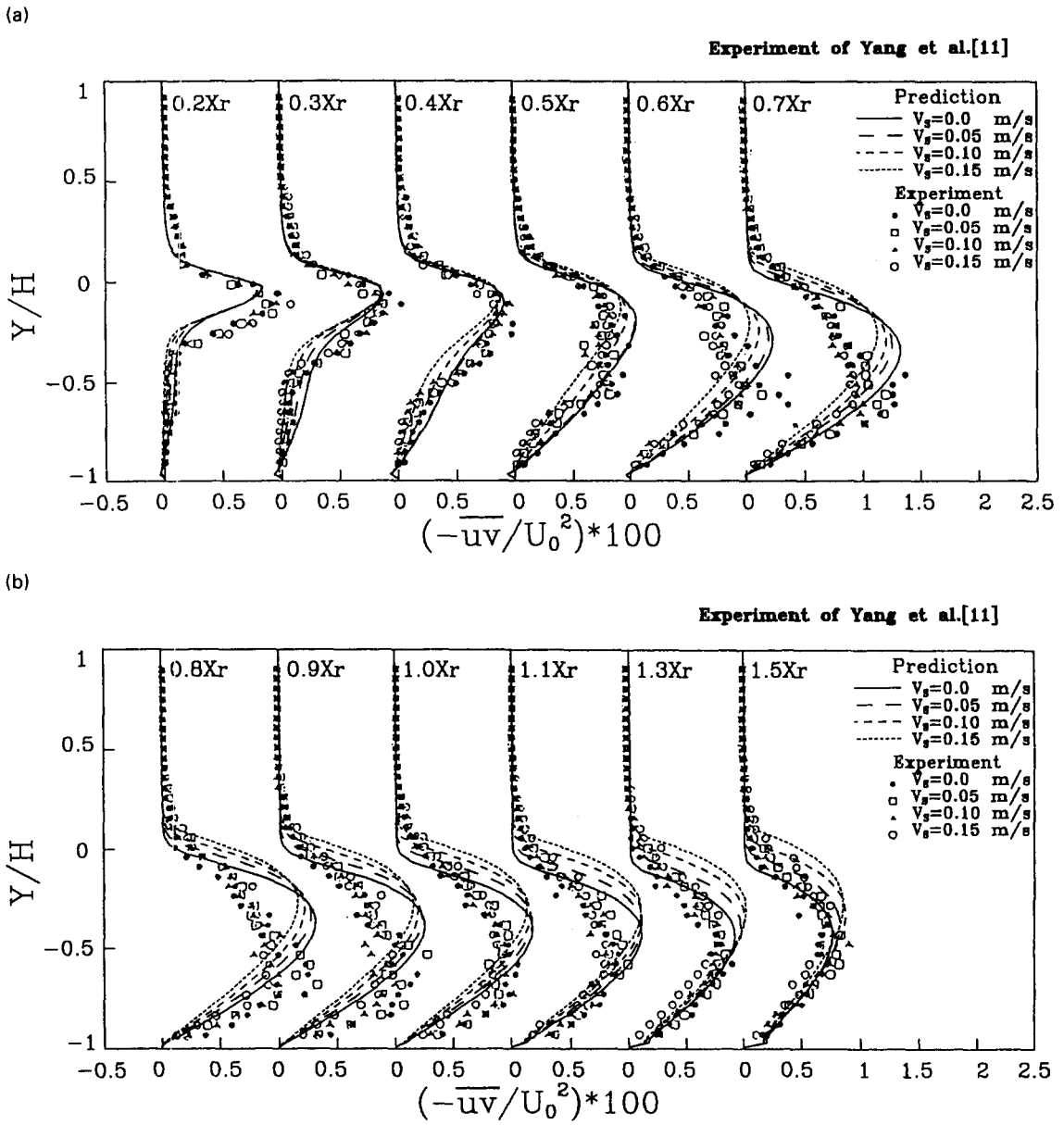

Fig. 10. Effects of the normal injection rate on Reynolds shear stress at $U_0 = 20$ m s^{-1} (a) $X/Xr = 0.2, 0.3, 0.4, 0.5, 0.6$ and 0.7; (b) $X/Xr = 0.8, 0.9, 1.0, 1.1, 1.3$ and 1.5.

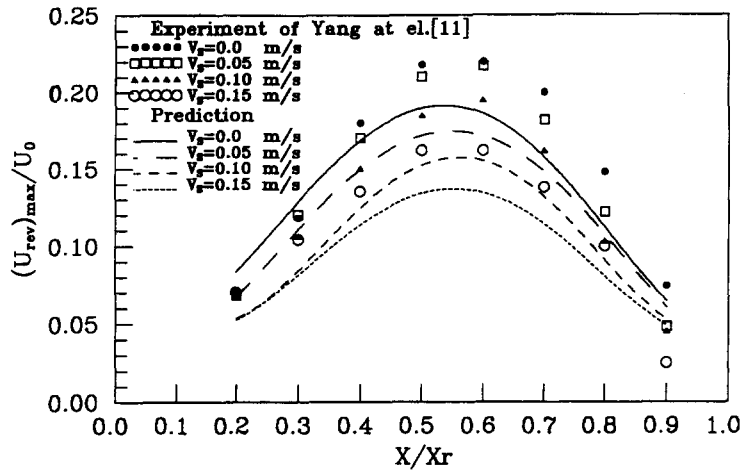

Fig. 11. Effect of the normal injection rate on the maximum reverse velocity at $U_0 = 20$ m s^{-1}.

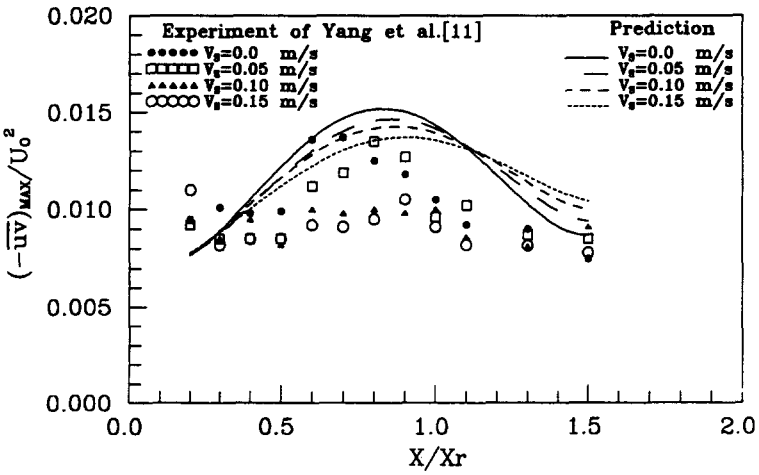

Fig. 12. Effect of the normal injection rate on the maximum Reynolds shear stress at $U_0 = 20$ m s^{-1}.

by the isotropic assumption in the eddy viscosity/diffusivity model and by the curvature effect.

REFERENCES

1. Abbort, D. E. and Kline, S. J., Experimental investigation of a subsonic turbulent flow over single and double backward facing steps. *ASME Journal of Basic Engineering*, 1962, **84,** 317.
2. Aung, W., An experimental study of laminar heat transfer downstream of backsteps. *ASME Journal of Heat Transfer*, 1983, **105,** 823–829.
3. Armaly, B. F., Durst, F., Pereira, J. C. F. and Schonung, B., Experimental and theoretical investigation of backward-facing step flow. *Journal of Fluid Mechanics*, 1983, **127,** 473–496.
4. Eaton, J. K. and Johnston, J. P., A review of research on subsonic turbulent flow reattachment. *AIAA Journal*, 1981, **19,** 1093–1100.
5. Kim, J., Kline, S. J. and Johnston, J. P., Investigation of a reattaching turbulent shear layer: flow over a backward-facing step. *ASME Journal of Fluids Engineering*, 1980, **102,** 302–308.
6. Schetz, J. A. and Nerney, B., Turbulent boundary layer with injection and surface roughness. *AIAA Journal*, 1977, **15,** 1288–1293.
7. Groot, W. A., Laser Doppler diagnostics of the flow behind a backward-facing step. Ph.D. thesis, Georgia Institute of Technology, 1985.
8. Lin, J. T., Armaly B. F. and Chen, T. S., Mixed convection in buoyancy-assisting, vertical backward-facing step flows. *International Journal of Heat and Mass Transfer*, 1990, **33,** 2121–2132.
9. Isomoto, K. and Honami, S., The effect of inlet turbulence intensity on the reattachment process over a backward-facing step. *ASME Journal of Fluids Engineering*, 1989, **111,** 87–92.
10. Oyakawa, K., Koike, T. and Mabuchi, I., Studies of heat transfer control by using jet discharge at reattachment region downstream of a backward-facing step. *JSME*, 1993, **59,** 543–549.
11. Yang, J. T., Tsai, B. B. and Tsai, G. L., Separated-reattaching flow over a backstep with uniform normal mass bleed. *ASME Journal of Fluids Engineering*, 1994, **116,** 29–35.
12. Launder, B. E. and Spalding, D. B., The numerical computation of turbulent flows. *Computer Methods in Applied Mechanical Engineering*, 1974, **3,** 269–289.
13. Abe, K., Kondoh, T. and Nagano, Y., A new turbulence model for predicting fluid flow and heat transfer in separating and reattaching flows. *International Journal of Heat and Mass Transfer*, 1994, **37,** 139–151.
14. P. Bradshaw, *Turbulence*. Springer, Berlin, 1976.
15. Patankar, S. V., *Numerical Heat Transfer and Fluid Flow*, Chaps 5–6. McGraw-Hill, New York, 1980, pp. 79–138.